Three-dimensional structure of the bacterial protein-translocation complex SecYEG

Cécile Breyton*†, Winfried Haase*, Tom A. Rapoport‡, Werner Kühlbrandt* & Ian Collinson*‡

** Max-Planck-Institut für Biophysik, Abteilung Strukturbiologie, Heinrich-Hoffmann-Straße 7, 60528 Frankfurt am Main, Germany*
‡ Department of Cell Biology, Harvard Medical School, 240 Longwood Avenue, Boston, Massachusetts 02115, USA
† Permanent address: CNRS-UMR7099, IBPC, 13 rue P. et M. Curie, 75005 Paris, France

Transport and membrane integration of polypeptides is carried out by specific protein complexes in the membranes of all living cells. The Sec transport path provides an essential and ubiquitous route for protein translocation[1]. In the bacterial cytoplasmic membrane, the channel is formed by oligomers of a hetero-trimeric membrane protein complex consisting of subunits SecY, SecE and SecG[2,3]. In the endoplasmic reticulum membrane, the channel is formed from the related Sec61 complex[4]. Here we report the structure of the *Escherichia coli* SecYEG assembly at an in-plane resolution of 8 Å. The three-dimensional map, calculated from two-dimensional SecYEG crystals, reveals a sandwich of two membranes interacting through the extensive cytoplasmic domains. Each membrane is composed of dimers of SecYEG. The monomeric complex contains 15 transmembrane helices. In the centre of the dimer we observe a 16 × 25 Å cavity closed on the periplasmic side by two highly tilted transmembrane helices. This may represent the closed state of the protein-conducting channel.

The fundamental mechanism underlying protein translocation through membranes cannot be understood without detailed information of the three-dimensional (3D) structure of the membrane proteins that form the translocation channel. So far, structural information has been limited to electron microscopy and single-particle analysis of the eukaryotic Sec61 or bacterial SecYEG complexes at low resolution[5–8]. To obtain a higher-resolution structure, crystalline membrane vesicles of the *E. coli* SecYEG were grown[9]. These crystals form by incorporation of the purified, detergent-solubilized complex into a phospholipid bilayer by slow removal of the detergent in the presence of lipids. This method has yielded SecYEG active in protein translocation[2,3,9]. The 3D structure of SecYEG was determined by the analysis of electron micrographs of crystals, tilted at angles of 0–55°. Amplitudes and phases of structure factors extracted from the images were combined to calculate a 3D map of SecYEG at 8 Å resolution in the membrane plane (Table 1, Fig. 1).

A side view of the map shows an unusual feature of the SecYEG crystals: they are composed of two membrane layers related to one another by a two-fold screw (2_1) axis (Fig. 1a). Therefore, the projection map[9] was a superposition of two crystalline membranes. This explains why it did not reveal the boundaries of the complex or its oligomeric state. The two membranes are each about 40 Å thick and separated by a zone of lower density roughly 25 Å wide. As each membrane layer contains only the noncrystallographic two-fold symmetry, the complexes within one membrane have the same orientation, and thus, owing to the crystallographic 2_1 axis, the two outer surfaces of the sandwich crystal are the same. The orientation of the protein in the crystals was investigated by immuno-electron microscopy, employing antibodies directed against the carboxy-terminal region of SecG or SecY, which are known to be located on the periplasmic and cytoplasmic sides of the membrane, respectively[10,11] (Fig. 2a, b). The SecG antibodies labelled the crystals, whereas the SecY antibodies did not (Fig. 2c, e). Thin sections of the crystals revealed that the SecG antibodies bound to both sides

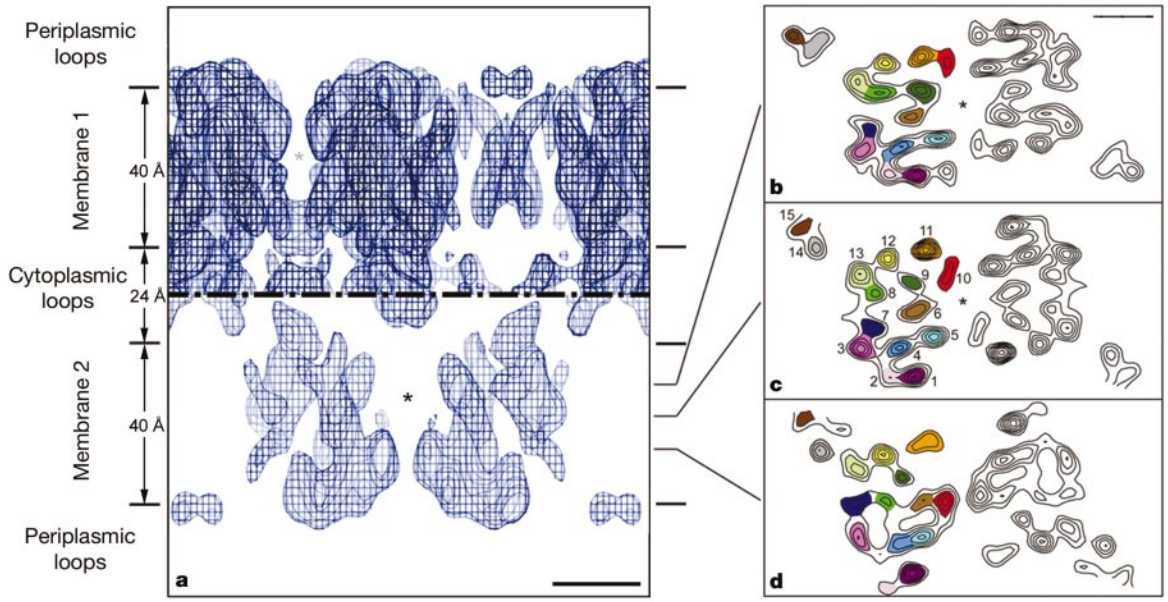

Figure 1 Double membrane crystal of SecYEG. **a**, Side view of the map of SecYEG at 8 Å in-plane resolution, with applied noncrystallographic two-fold symmetry, contoured at 1.35 s.d. A region of lower density, containing the cytoplasmic loops from both layers, separates the two membranes. The membranes are related to one another by the crystallographic 2_1 axis. The upper membrane is a slab one-unit cell deep. The lower membrane is a thinner slab centred on the two-fold axis of the dimer, revealing a putative channel (asterisk), which is closed on the periplasmic side. **b**–**d**, Horizontal sections, 8 Å apart, through the SecYEG dimer, as indicated in **a**. In each section, 15 peaks of density, corresponding to sections of membrane-spanning helices, are resolved within a monomer of SecYEG. They are arbitrarily numbered from 1 to 15 and colour coded. Scale bar, 20 Å.

of the double membrane (Fig. 2d). Therefore, the outer surfaces of the crystal correspond to the periplasmic side of the protein, and the more extensive cytoplasmic domains provide the crystal contacts between the two membranes (Fig. 1a). These features are consistent with topology models indicating that twice as many residues of SecYEG are exposed on the cytoplasmic surface than on the periplasmic side[10,11].

Within a single membrane, the SecYEG complex forms dimers that are clearly separated from one another by featureless, lipid-containing regions (Fig. 3a). The two monomers within the dimer are related to each other by noncrystallographic two-fold symmetry. In each SecYEG monomer, 15 rod-shaped densities—characteristic of membrane-spanning α-helices—are resolved (arbitrarily labelled 1–15; Figs 1b–d and 3), consistent with predictions based on polypeptide hydropathy. Helices 1, 3 and 12 run roughly perpendicular to the membrane plane; helices 2, 4, 6, 11 and 13–15 have tilt angles of 5–20° relative to the membrane normal, whereas helices 5 and 7–10 are highly tilted by 30–45° (Fig. 3a). All membrane-spanning helices are well resolved at a contour level of one s.d. (Figs 1b–d and 3).

The monomer accommodates 13 tightly packed helices, with centre-to-centre distances of 7–13 Å. The two remaining helices are isolated from the main bundle. SecY, SecE and SecG are predicted to contain 10, 3 and 2 membrane-spanning α-helices, respectively. Because SecG is not required for translocation *in vitro*[2,12] or *in vivo*[13], a peripheral location of this subunit in the complex seems likely. Therefore, helices 14 and 15 may correspond to SecG. The remaining 13 helices can be described in terms of a central four-helix bundle (tilted helices 6–9) with a left-handed twist, surrounded by three other groups: a layer of less tilted helices (11–13) on one side, a right-handed four-helix bundle (helices 1–4) on the opposite side, and two highly tilted helices (5 and 10) at the dimer interface (Fig. 3a).

In the centre of the SecYEG dimer there is a clear cavity 16 × 25 Å wide and 22 Å deep around the position of the noncrystallographic two-fold axis (asterisk in Fig. 1). This indentation is closed on the periplasmic membrane surface (Fig. 1), and is formed at the interface of the two monomers. The cavity is lined by the whole length of helices 5 and 10 and, on the cytoplasmic half, also by helices 6 and 9. The highly tilted helix 10 is in close contact with the same helix of the adjacent monomer on the periplasmic membrane side. These two helices tilt away from one another towards the cytoplasmic side in a V-shaped configuration (Fig. 3a, b), closing the cavity on the periplasmic side.

Our map shows that a single SecYEG monomer does not contain a channel that would be large enough for protein translocation. Consistent with this result, most studies of SecYEG and Sec61p suggest that the translocation channel is formed by an assembly of several copies of the translocase complex, although the exact stoichiometry is uncertain. A recent analysis found that translocating protein is associated with a dimer of SecYEG[14], but trimers[7] and tetramers[5,8] have also been proposed to form the translocation conduit. All these studies suggest, however, that the channel is

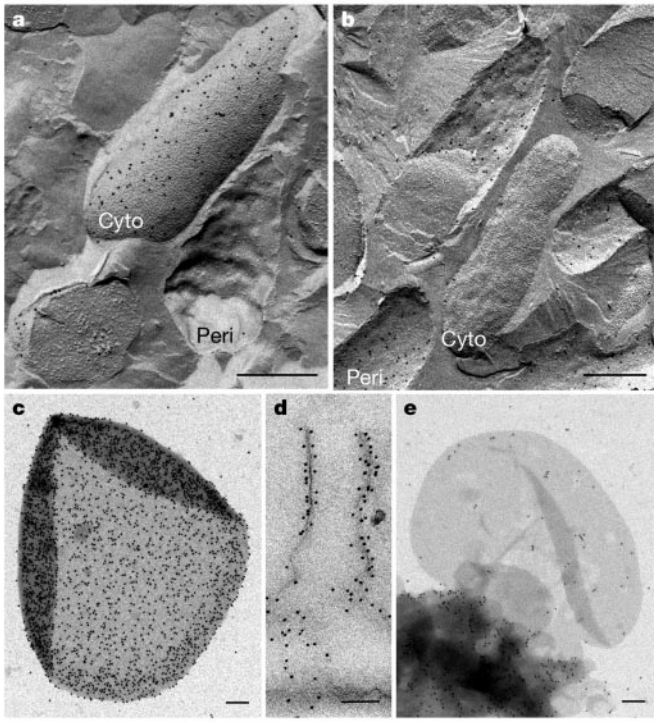

Figure 2 Immunogold labelling with antibodies directed against C-terminal fragments of SecG (**b**–**d**) or of SecY (**a** and **e**). *E. coli* cells overexpressing the SecYEG complex were freeze-fractured, splitting the inner membrane into convex (cytoplasmic, cyto) and concave (periplasmic, peri) leaflets. Immunogold labelling was performed as described[24]. As expected, the SecG antibodies labelled only the periplasmic surface (**b**), whereas the SecY antibodies bound only to the cytoplasmic surface of the bacterial membrane (**a**). SecYEG crystals were immunogold labelled on the electron microscope grid support film (**c** and **e**) or adsorbed to plastic slides before embedding and thin sectioning (**d**). In either case, only periplasmic epitopes were labelled, indicating that both faces of the two-dimensional crystals correspond to the periplasmic surface of the complex. Scale bars: **a**, **b**, 500 nm; **c**–**e**, 200 nm.

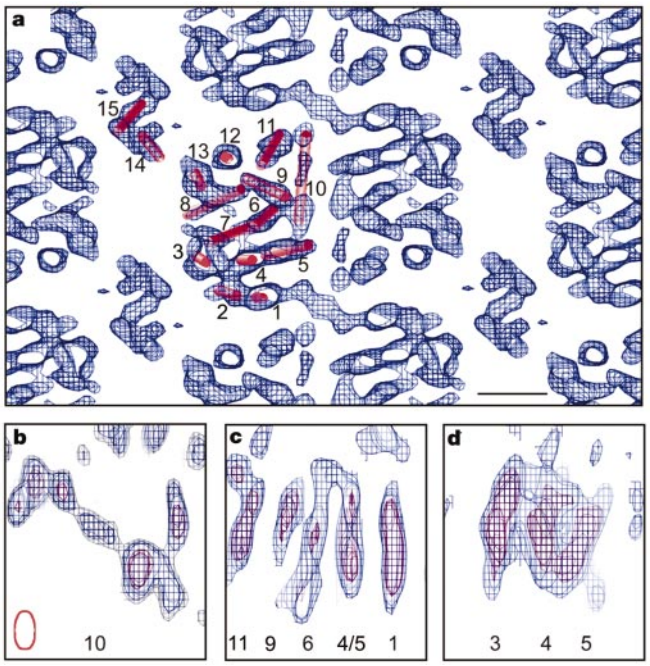

Figure 3 Dimeric structure of the SecYEG complex. **a**, Top view from the cytoplasmic side of one crystalline membrane with applied two-fold noncrystallographic symmetry. The unsymmetrized map and the electron density file (as a brk input to the program O[30]) are available as Supplementary Information. SecYEG dimers are clearly separated from one another. Within one monomer, the 15 transmembrane helices are drawn as red cylinders. The two peripheral helices, 14 and 15, may correspond to the non-essential SecG subunit. **b**–**d**, Side views of helices contoured at 1.0 (grey; in **b** only), 1.35 (blue) and 2.7 (pink) s.d. In **c**, tilted helix 9 extends outside the slab. All helix densities are continuous at one s.d. At increasing contour levels, the densities of the most highly tilted helices, 10 and 7, appear discontinuous, as expected owing to the missing cone of data. The anisotropy of the resolution is illustrated by the elongation of the point spread function along the direction perpendicular to the membrane plane[28] (red inset in **b**).

Table 1 **Crystallographic data summary**

Plane group symmetry	$p12_{1}$-b
Unit cell dimensions	$a = 104$ Å, $b = 57$ Å, $\gamma = 90°$
Thickness	~120 Å
Number of lattices*	63
Total no. of observations†	6,213
No. of unique structure factors‡	2,175
Overall weighted phase error†‡§	20.3°

*Distribution of tilt angles: 0–10°, 17 images; 10–20°, 8 images; 20–30°, 6 images; 30–40°, 26 images; 40–55°, 6 images.
†Including reflections with signal-to-noise ratios greater than one (IQ 1–8; ref. 25).
‡Before imposing the noncrystallographic symmetry.
§90° is random.

located at the interface between monomers. Our map of the SecYEG dimer shows a deep cavity at the dimer interface that is closed at the periplasmic side of the membrane. This may be the closed translocation channel. The diameter of the cavity is similar to that of previously observed translocation pores, ranging from 9 to 25 Å (refs 5, 7, 8). Furthermore, the most recent map of a ribosome-associated Sec61 channel also displays a central indentation rather than a continuous channel, and is closed on the side of the membrane that would correspond to the periplasmic surface[7]. Small conformational changes would be sufficient to convert the observed cavity into a continuous channel: the helices 10 of adjacent monomers could move away from one another to facilitate protein translocation. Helix 10 could correspond to the conserved third transmembrane domain of SecE, which has been shown to be a contact site between two monomers[15] and is thought to have a dynamic role in protein translocation[15–18]. However, we cannot exclude the possibility that the active channel is formed upon incorporation of additional SecYEG monomers into the oligomeric complex[8]. Irrespective of the mechanism of channel formation, the dimer we find in the membrane crystals could represent a state of the SecYEG complex that can initiate protein translocation. Therefore, it would contain the binding sites for SecA and for the signal sequence of a translocation substrate. SecA is an ATPase that delivers the protein substrate to the channel and is thought to move in and out of a SecYEG structure while being shielded from phospholipid[19–21]. This interaction results in a progressive movement of the polypeptide through the pore[19,20]. SecA could be bound by the extensive cytosolic loops of the SecYEG complex near the dimer interface. The cavity is too small to enclose the entire SecA dimer, which measures about 150 × 80 × 80 Å (ref. 22), suggesting that only a part of SecA inserts into the channel, or that additional SecYEG molecules combine to engulf SecA. The cavity we observe would provide an easy route for the signal sequence to proceed from SecA to then intercalate between the SecY transmembrane helices[17] and thus to initiate protein translocation. □

Methods

Antibody labelling

On-grid and pre-embedding immunogold labelling were performed as described[23]. Antibodies were raised against synthetic peptides corresponding to the last 15 and 16 amino acids of SecY and SecG, respectively, plus additional cysteines at the amino terminus. The sequences chosen, according to topology predictions, correspond to both periplasmic (SecG) and cytoplasmic (SecY) regions of the complex. The binding sites of the antibodies with respect to the plasma membrane were confirmed by freeze-fracture replica labelling of whole cells[24] (Fig. 2a, b).

Data collection, processing and analysis

Two-dimensional crystals of SecYEG were obtained and imaged by electron cryomicroscopy as described[9]. Images recorded at 0, 20, 30 or 45° nominal tilt were evaluated by optical diffraction. Well-ordered areas of 4,000 × 4,000 pixels were digitized on a Zeiss SCAI scanner with a 7-μm step. Images were corrected for distortion of the crystal lattice, the effects of the contrast transfer function (CTF) and astigmatism using the MRC image-processing programs[25,26]. Initial estimates of tilt angles were calculated from lattice parameters, and amplitudes and phases of structure factors were merged in plane group $p12_1$. The absolute hand of the map was checked with an image of tilted purple membrane, which was compared to the bacteriorhodopsin 3D data set[27]. The phase origin, tilt geometry and CTF of each image were refined. About 70 of ~2,000 images yielded 8–10 Å data, and 63 lattices were merged. The vertical resolution was estimated at ~16 Å by the point-spread function[28]. Image amplitudes were scaled with an average temperature factor of −600 Å^2 to compensate for resolution-dependent drop-off. The 3D density map was calculated with CCP4 programs[29], and the map displayed with the program O[30]. The two-fold noncrystallographic symmetry was determined by the CCP4 program FINDNCS and applied using the program MAPROT.

Received 11 March; accepted 18 April 2002; doi:10.1038/nature00827.

1. Matlack, K., Mothes, W. & Rapoport, T. Protein translocation: tunnel vision. *Cell* **92,** 381–390 (1998).
2. Brundage, L., Hendrick, J. P., Schiebel, E., Driessen, A. J. & Wickner, W. The purified *E. coli* integral membrane protein SecY/E is sufficient for reconstitution of SecA-dependent precursor protein translocation. *Cell* **62,** 649–657 (1990).
3. Akimaru, J., Matsuyama, S. I., Tokuda, H. & Mizushima, S. Reconstitution of a protein translocation system containing purified SecY, SecE, and SecA from *Escherichia coli*. *Proc. Natl Acad. Sci. USA* **88,** 6545–6549 (1991).
4. Gorlich, D., Prehn, S., Hartmann, E., Kalies, K. & Rapoport, T. A. A mammalian homolog of SEC61p and SECYp is associated with ribosomes and nascent polypeptides during translocation. *Cell* **71,** 489–503 (1992).
5. Hanein, D. *et al.* Oligomeric ring of the Sec61p complex induced by ligands required for protein translocation. *Cell* **87,** 721–732 (1996).
6. Ménétret, J.-F. *et al.* The structure of ribosome–channel complexes engaged in protein translocation. *Mol. Cell* **6,** 1219–1232 (2000).
7. Beckmann, R. *et al.* Architecture of the protein-conducting channel associated with the translocating 80S ribosome. *Cell* **107,** 361–372 (2001).
8. Manting, E., van der Does, C., Remigy, H., Engel, A. & Driessen, A. J. M. SecYEG assembles into a tetramer to form the active protein translocation channel. *EMBO J.* **19,** 852–861 (2000).
9. Collinson, I. *et al.* Projection structure and oligomeric properties of a bacterial core protein translocase. *EMBO J.* **20,** 2462–2471 (2001).
10. Nishiyama, K., Suzuki, T. & Tokuda, H. Inversion of the membrane topology of SecG coupled with SecA-dependent preprotein translocation. *Cell* **85,** 71–81 (1996).
11. Akiyama, Y. & Ito, K. Topology analysis of the SecY protein, an integral membrane protein involved in protein export in *Escherichia coli*. *EMBO J.* **6,** 3465–3470 (1987).
12. Duong, F. & Wickner, W. Distinct catalytic roles of the SecYE, SecG and SecDFyajC subunits of preprotein translocase holoenzyme. *EMBO J.* **16,** 2756–2768 (1997).
13. Nishiyama, K., Hanada, M. & Tokuda, H. Disruption of the gene encoding p12 (SecG) reveals the direct involvement and important function of SecG in the protein translocation of *Escherichia coli* at low temperature. *EMBO J.* **13,** 3272–3277 (1994).
14. Bessonneau, P., Besson, V., Collinson, I. & Duong, F. The SecYEG preprotein translocation channel is a conformationally dynamic and dimeric structure. *EMBO J.* **21,** 995–1003 (2002).
15. Kaufmann, A., Manting, E. H., Veenendaal, A. K., Driessen, A. J. & van der Does, C. Cysteine-directed cross-linking demonstrates that helix 3 of SecE is close to helix 2 of SecY and helix 3 of a neighbouring SecE. *Biochemistry* **38,** 9115–9125 (1999).
16. Flower, A. M., Osborne, R. S. & Silhavy, T. J. The allele-specific synthetic lethality of prlA-prlG double mutants predicts interactive domains of SecY and SecE. *EMBO J.* **14,** 884–893 (1995).
17. Plath, K., Mothes, W., Wilkinson, B. M., Stirling, C. J. & Rapoport, T. A. Signal sequence recognition in posttranslational protein transport across the yeast ER membrane. *Cell* **94,** 795–807 (1998).
18. Veenendaal, A. K., van der Does, C. & Driessen, A. J. Mapping the sites of interaction between SecY and SecE by cysteine scanning mutagenesis. *J. Biol. Chem.* **276,** 32559–32566 (2001).
19. Economou, A. & Wickner, W. SecA promotes preprotein translocation by undergoing ATP-driven cycles of membrane insertion and deinsertion. *Cell* **78,** 835–843 (1994).
20. van der Wolk, J. P., de Wit, J. G. & Driessen, A. J. The catalytic cycle of the *Escherichia coli* SecA ATPase comprises two distinct preprotein translocation events. *EMBO J.* **16,** 7297–7304 (1997).
21. Eichler, J., Brunner, J. & Wickner, W. The protease-protected 30 kDa domain of SecA is largely inaccessible to the membrane lipid phase. *EMBO J.* **16,** 2188–2196 (1997).
22. Shilton, B. *et al. Escherichia coli* SecA shape and dimensions. *FEBS Lett.* **436,** 277–282 (1998).
23. Kleymann, G., Ostermeier, C., Heitmann, K., Haase, W. & Michel, H. Use of antibody fragments (Fv) in immunocytochemistry. *J. Histochem. Cytochem.* **43,** 607–614 (1995).
24. Fujimoto, K. SDS-digested freeze-fracture replica labeling electron microscopy to study the two-dimensional distribution of integral membrane proteins and phospholipids in biomembranes: practical procedure, interpretation and application. *Histochem. Cell Biol.* **107,** 87–96 (1997).
25. Henderson, R., Baldwin, J. M., Downing, K. H. & Zemlin, F. Structure of purple membrane from *Halobacterium halobium*. Recording, measurement and evaluation of electron micrographs at 3.5 Å resolution. *Ultramicroscopy* **19,** 147–178 (1986).
26. Crowther, R. A., Henderson, R. & Smith, J. M. MRC image processing programs. *J. Struct. Biol.* **116,** 9–16 (1996).
27. Grigorieff, N., Ceska, T. A., Downing, K. H., Baldwin, J. M. & Henderson, R. Electron-crystallographic refinement of the structure of bacteriorhodopsin. *J. Mol. Biol.* **259,** 393–421 (1996).
28. Unger, V. M. Assessment of electron crystallographic data obtained from two-dimensional crystals of biological specimens. *Acta Crystallogr. D* **56,** 1259–1269 (2000).
29. Collaborative Computational Project No. 4. The CCP4 suite: programs for protein crystallography. *Acta Crystallogr. D* **50,** 760–763 (1994).
30. Jones, T. A., Zou, J. Y., Cowans, S. W. & Kjeldgaard, M. Improved methods for building protein models in electron density maps. *Acta Crystallogr.* **47,** 110–119 (1991).

Supplementary Information accompanies the paper on *Nature*'s website (http://www.nature.com/nature).

Acknowledgements

We thank E. Or for the production of the polyclonal antibodies, F. Joos for immunostaining of thin sections, and F. Duong for critically reading the manuscript. C.B. is grateful to D. Mills for help with the JEOL3000SFF electron microscope, V. Unger for advice on image processing, J. Vonck for discussions on noncrystallographic symmetry, and D. Picot for discussions and advice on crystallographic programs. I.C. was a fellow of

the Human Frontiers Science Program at Harvard University. C.B. acknowledges support from Jean-Luc Popot and the CNRS-UMR7099, where she carried out the final part of the analysis.

Competing interests statement

The authors declare that they have no competing financial interests.

Correspondence and requests for materials should be addressed to C.B. (e-mail: Cecile.Breyton@ibpc.fr) or I.C. (e-mail: Ian.Collinson@mpibp-frankfurt.mpg.de).

corrigendum

Extensive and divergent circadian gene expression in liver and heart

Kai-Florian Storch, Ovidiu Lipan, Igor Leykin, N. Viswanathan, Fred C. Davis, Wing H. Wong & Charles J. Weitz

Nature **417**, 78–83 (2002).

Two errors of gene annotation have come to our attention. Although we refer to *Zfp36* in the text, the gene identified in our data sets was *Zfp36l-1* (*Zfp36-like 1*; NCBI RefSeq accession number NM_007564). Current evidence suggests that *Zfp36l-1* protein and its close relatives are RNA-binding factors rather than transcription factors[1–3]. Rather than *Thra* (thyroid hormone receptor-α), which we identified on the basis of an incorrect Unigene cluster assignment in NCBI, the correct assignment is the nuclear orphan receptor *Rev-erb-β* (GenBank accession number U09504). These corrections do not affect our conclusions in any significant way.

1. Carballo, E., Lai, W. S. & Blackshear, P. J. Feedback inhibition of macrophage tumor necrosis factor-alpha production by tristetraprolin. *Science* **281,** 1001–1005 (1998).
2. Lai, W. S. *et al.* Evidence that tristetraprolin binds to AU-rich elements and promotes the deadenylation and destabilizatuion of tumor necrosis factor alpha mRNA. *Mol. Cell Biol.* **19,** 4311–4323 (1999).
3. Lai, W. S., Carballo, E., Thorn, J. M., Kennington, E. A. & Blackshear, P. J. Interactions of CCCH zinc finger proteins with mRNA. Binding of tristetraprolin-related zinc finger proteins to Au-rich elements and destabilization of mRNA. *J. Biol. Chem.* **275,** 17827–17837 (2000).

addendum

Nitrogen loss from unpolluted South American forests mainly via dissolved organic compounds

Steven S. Perakis & Lars O. Hedin

Nature **415**, 416–419 (2002).

In this Letter we reported that hydrologic export of dissolved organic nitrogen (DON) dominates over nitrate in unpolluted old-growth forests across southern Chile and Argentina, but that the reverse pattern occurs in old-growth forests exposed to chronically high rates of nitrogen deposition in eastern North America. As a note of clarification, however, we feel it is useful to point out that, depending on conditions, second-growth forests (that is, those that have been previously logged) can display various patterns of nitrogen loss, including dominance of DON over nitrate[1,2] in cases where forest regrowth and detritus accumulation exert strong and well-known demands on internal nitrate supply[3–6]. But these forests were not included in our analysis, given that their nitrogen cycles are influenced by historically complex interactions between nitrogen deposition and land use and so do not represent an appropriate comparison to the old-growth forests investigated in South America.

1. Goodale, C. L., Aber, J. D. & McDowell, W. H. The long-term effects of disturbance on organic and inorganic nitrogen export in the White Mountains, New Hampshire. *Ecosystems* **3,** 433–450 (2000).
2. Campbell, J. L. *et al.* Dissolved organic nitrogen budgets for upland, forested ecosystems in New England. *Biogeochemistry* **49,** 123–142 (2000).
3. Vitousek, P. M. & Reiners, W. A. Ecosystem succession and nutrient retention: a hypothesis. *BioScience* **25,** 376–381 (1975).
4. Hedin, L. O., Armesto, J. J. & Johnson, A. H. Patterns of nutrient loss from unpolluted, old-growth temperate forests: evaluation of biogeochemical theory. *Ecology* **76,** 493–509 (1995).
5. Likens, G. E. & Bormann, F. H. *Biogeochemistry of a Forested Ecosystem* 2nd edn (Springer, New York, 1995).
6. Aber, J. D. *et al.* Nitrogen saturation in temperate forest ecosystems: Hypotheses revisited. *BioScience* **48,** 921–934 (1998).